Volume 55
Number 3
20 January 2026
Pages 995-1502

Dalton Transactions

An international journal of inorganic chemistry

rsc.li/dalton

ISSN 1477-9226

ROYAL SOCIETY OF **CHEMISTRY**

PAPER
Ravinder Pawar *et al.*
Can silaborane serve as an effective bridging unit for Lewis pairs? A comparative discourse with carborane

Dalton Transactions

PAPER

View Article Online
View Journal | View Issue

Cite this: *Dalton Trans.*, 2026, **55**, 1125

Can silaborane serve as an effective bridging unit for Lewis pairs? A comparative discourse with carborane

Mohmmad Faizan, Zaid Malik, Madem Sandhya and Ravinder Pawar *

Frustrated Lewis pairs (FLPs) have emerged as versatile metal-free catalysts for small-molecule activation, and strategies to control frustration through geometric immobilization and electronic tuning remain a topic of significant interest. Carborane cages, with their unique coordination-dependent electronic effects, have recently been shown to modulate FLP frustration. In this work, we introduce *o*-silaborane cages, whose coordination-based electronic effects had not previously been explored for modulating FLP reactivity. The $-BH_2$ and $-PH_2$ substituents were strategically placed at distinct coordinating sites of the cages to systematically compare the coordination dichotomy of *o*-carborane and *o*-silaborane frameworks in influencing the frustration of Lewis pairs. CO_2 activation was employed as the model reaction to assess and compare these effects. Electronic structure analysis reveals that silaborane exerts stronger electron-withdrawing and electron-donating influences than carborane, leading to pronounced differences in acidity–basicity balance, strain distribution, and the stability of CO_2 complexes. Furthermore, transition-state energetics demonstrate that site-dependent positioning of Lewis acid–base centres critically governs activation barriers. In the *o*-carborane framework, the acid and base groups positioned at the 1,4-sites exhibit the highest reactivity, whereas in the *o*-silaborane system, the 4,9-substituted arrangement is identified as the most reactive. These findings establish silaborane as a promising bridging unit, opening new design pathways for tuneable FLP-based CO_2 utilization and broader small-molecule activation.

Received 6th October 2025,
Accepted 4th December 2025

DOI: 10.1039/d5dt02382c

rsc.li/dalton

Introduction

The emergence of frustrated Lewis pair (FLP) catalysis following the successful activation of molecular hydrogen[1] has opened new avenues for the development of metal-free catalysts for small-molecule activation. Since then, a wide variety of inter- and intramolecular FLPs have been designed and investigated.[2–24] In addition to creating new FLPs, significant efforts have focused on controlling their reactivity through geometric immobilization of the active sites using bridging units, as well as through electronic modulation of acidity and basicity by introducing electron-withdrawing or electron-donating substituents.[25,26] Such structural and electronic modifications can provide improved thermodynamic and kinetic control in FLP-mediated catalysis. A notable contribution by Trujillo and Fernández demonstrated the effect of aromatic modifications on FLP reactivity, highlighting the role of electronic perturbations.[27,28] Building on this, our recent work employed orbital analysis and metadynamics simulations to further elucidate how different electron-donating and -withdrawing scenarios alter the reaction pathways.[29,30] Beyond electronic effects, the spatial arrangement of the acidic and basic centers has also been shown to be critical.[31,32] Intramolecular FLPs (IFLPs), in which the active sites are immobilized at appropriate distances and angles by bridging units, have displayed enhanced reactivity toward CO_2.[31–33] For example, Dang and co-workers systematically examined P/B-based IFLPs for CO_2 hydrogenation, revealing that unsaturated and extended bridging frameworks provide favorable geometrical parameters for higher turnover frequencies.[34] Considering both ways to control the frustration of the FLPs, the search for such bridging unit that can provide appropriate geometrical immobilization of the active sites along with the suitable electronic effects is underexplored.

In this context, *o*-carborane, a twelve-vertex icosahedral, neutral carbon–boron cluster (Fig. 1a), emerges as an exceptional bridging scaffold owing to its remarkable stability and coordination-dependent electronic properties, often described as *coordination dichotomy*.[35–37] Since its first report in 1963,[38,39] experimental studies have established *o*-carborane as an electron-deficient polyhedral cluster composed of triangular faces formed through three-centre–two-electron (3c–2e) bonds. The cage exhibits three-dimensional aromaticity arising from electron delocalization over the entire

Laboratory of Advanced Computation and Theory for Materials and Chemistry, Department of Chemistry, National Institute of Technology Warangal (NITW), Warangal, Telangana 506004, India. E-mail: ravinder_pawar@nitw.ac.in

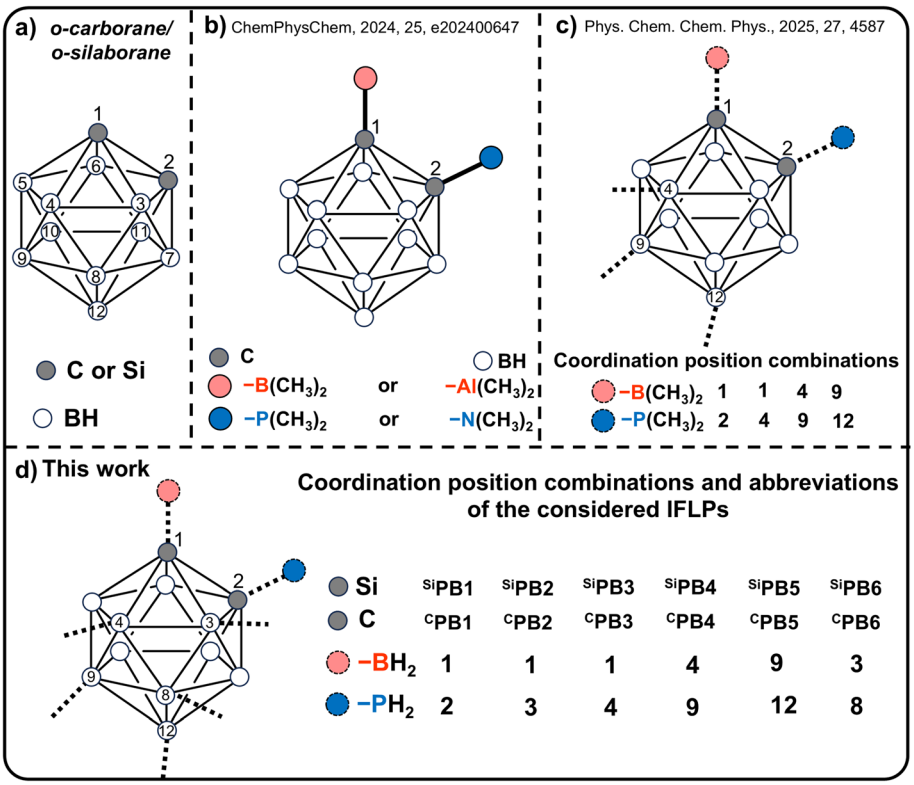

Fig. 1 (a) General structure of *o*-carborane and *o*-silaborane, (b) *o*-carborane-based intramolecular frustrated Lewis pairs (IFLPs) investigated for CO_2 sequestration; (c) coordination dichotomy of the carborane cage and its effect on IFLP frustration; (d) IFLPs examined in the present study, formed by different positional arrangements of $-PH_2$ and $-BH_2$ substituents on carborane and silaborane cages.

framework.[40–43] Importantly, this delocalization is non-uniform, imparting distinct electron densities at different atomic sites and thereby generating position-dependent electronic effects within the cluster. The acidity or basicity of substituents attached to the carborane polyhedron is directly governed by the electron density at the specific carbon or boron site of attachment.[43–46] The electron-density distribution in *o*-carborane follows the order C(1,2) < B(3,6) < B(4,5,7,11) < B(8,10) < B(9,12) (Fig. 1a), indicating that the cage carbon atoms exert strong electron-withdrawing effects, whereas the B9 and B12 vertices are strongly electron-donating.[43–46] Consequently, borane substitution at cage carbon sites generates highly acidic centres,[47] while phosphine substitution at boron sites antipodal to the carbon atoms yields strongly basic functionalities.[48,49] These inductive effects of C- and B-bound carboranyl groups were quantitatively described using inductive constants derived from ^{19}F NMR chemical-shift measurements of *para*- and *meta*-substituted fluorobenzenes by Taft method.[43,50,51] This distinct variation in electronic influence positions *o*-carborane as a highly versatile bridging unit capable of modulating electronic effects solely through the choice of coordination site. Such tunability is particularly advantageous for FLP chemistry, where controlling the degree of frustration is essential. Therefore, *o*-carborane based intramolecular FLPs are anticipated to display frustration that is inherently governed by the cage's coordination-dependent electronic dichotomy. Welch and co-workers in 2019 reported the first base- and acid-functionalized *o*-carborane, 1-Bcat-7-PPh_2-*closo*-1,7-$C_2B_{10}H_{10}$, although it was not considered as an IFLP due to insufficient geometrical requirements for frustration.[52] Subsequently, Xie and colleagues reported the first *o*-carborane IFLP, 1-PPh_2-2-BPh_2-1,2-$C_2B_{10}H_{10}$, which was shown to catalyze tri-insertion and dearomatization of terminal arylalkynes.[53] More recently, Zhu and co-workers theoretically investigated *o*-carborane-based IFLPs (*o*-IFLPs) for N_2 activation.[54] Despite these advances, the impact of coordination dichotomy on the degree of frustration in IFLPs has received relatively little attention. Building on these developments, we investigated *o*-IFLPs for CO_2 activation (Fig. 1b).[55] Furthermore, we demonstrated that the coordination dichotomy intrinsic to the carborane cage plays a decisive role in modulating the frustration and reactivity of the embedded Lewis pairs (Fig. 1c).[56] Collectively, these results highlight *o*-carborane frameworks as powerful and tunable bridging units for controlling FLP reactivity.

Analogous to *o*-carborane, the icosahedral 12-vertex silicon–boron cluster, *o*-silaborane (Fig. 1a), was first reported and examined by Seyferth and co-workers.[57,58] The reaction between $CH_3(H)Si(NMe_2)_2$ and $B_{10}H_{14}$ yielded 1,2-dimethyl-1,2-disila-*closo*-dodecaborane (*i.e.*, *o*-silaborane). The isolated *o*-silaborane exhibited chemical stability and did not react with $Me_3SiCl/AlCl_3$ or $Me_3SiCl/AlBr_3$ in either CH_2Cl_2 or

$CHCl_3$.[57,58] It was similarly unresponsive toward $HCl/AlCl_3$ and $HCl/AlBr_3$. In contrast, treatment with ethanolic KOH led to rapid and complete decomposition of the silaborane.[57,58]

Beyond the parent 1,2-dimethyl-1,2-disila-*closo*-dodecaborane *i.e.*, *o*-silaborane, a diverse family of derivatives has been reported. Substitution at the silicon vertices affords *closo* analogues such as the 1,2-diphenyl- and 1-methyl-2-phenyl-1,2-disila-*closo*-dodecaboranes, which retain the characteristic Si_2B_{10} cage geometry.[59] Controlled nucleophilic attack at the Si-localized LUMO leads to cage degradation, generating *nido* and *closo* silaborates including $[nido\text{-}(MeSi)B_{10}H_{12}]^-$ and $[closo\text{-}(MeSi)B_{11}H_{11}]^-$, as well as related *arachno*-type products.[60] The parent cluster also forms a variety of addition products such as amido-bridged species such as $[(Et_2N)(MeSi)_2B_{10}H_{10}]^-$ and corresponding Zr/Ta amido complexes;[59] alkoxide and oxo-bridged adducts including $[(TMPDAH)_2((Me_2Si_2B_{10}H_{10})_2O)]$ and $[TMPDAH][(Me_2Si_2B_{10}H_{10})OMe]$.[61] Collectively, these derivatives demonstrate the pronounced nucleophilicity and versatile reactivity imparted by the two adjacent silicon vertices, distinguishing *o*-silaborane chemistry from that of the isoelectronic *o*-carborane. Also, the He(I) photoelectron spectroscopic studies established that the *o*-silaborane cage is more electron rich than the corresponding carborane cage. This difference arises because the Si atom donates more electron density to the silaborane cage than the C atom donates in *o*-carborane, owing to the lower effective nuclear charge of Si relative to C. Consequently, the less electronegative Si atom transfers electron density more readily to the cage, making the boron atoms in *o*-silaborane more electron rich than those in the carborane cage, and correspondingly rendering Si more electron withdrawing than the cage carbon atoms of *o*-carborane. Thus, *o*-silaborane is expected to impart stronger electronic effects than *o*-carborane, and the frustration of silaborane-bridged Lewis pairs may differ from that of carborane-supported Lewis pairs. Moreover, to the best of our knowledge, the coordination-dependent electronic effects of *o*-silaborane remain unexplored and have not been correlated with those of carborane, particularly in the context of IFLP frustration. This gap provides an opportunity to examine the coordination dichotomy of *o*-silaborane and to evaluate its potential as a bridging unit for IFLPs.

The present study aims to comparatively investigate the coordination dichotomy of *o*-silaborane and *o*-carborane in modulating Lewis-pair frustration. To this end, $-PH_2$ and $-BH_2$ groups were introduced at different coordination sites of both cages to generate a series of IFLPs (Fig. 1d), which were subsequently analyzed for CO_2 activation to determine how variations in coordination sites influence reactivity. The use of $-PH_2$ and $-BH_2$ substituents allows us to isolate the electronic influence of the cages on frustration without introducing additional steric or electronic contributions from the substituents themselves. Furthermore, for the most favourable coordination sites of both cages, the reactivity of $-PH_2/-B(CF_3)_2$ and $-P(CH_3)_2/-B(CF_3)_2$ Lewis acid–base pairs was also examined. Overall, this study elucidates the coordination dichotomy of *o*-silaborane and assesses its suitability as a bridging scaffold for IFLPs, while laying the foundation for future work on catalytic CO_2 conversion into value-added products.

Computational details

The structures of the considered *o*-carborane- and *o*-silaborane-based IFLPs, their corresponding reactant complexes (CMs), transition states (TSs), and the formed CO_2 adducts were fully optimized without any geometric or symmetry constraints using the ωB97X-D functional in combination with the 6-311++G** basis set.[62,63] Harmonic frequency calculations were performed at the same level of theory to confirm the nature of the stationary points, identifying local minima and first-order saddle points. Transition states were validated by the presence of a single imaginary frequency corresponding to the expected bond reorganization. Intrinsic reaction coordinate (IRC) analyses were further carried out to ensure that the identified TSs connect the appropriate reactants and products. All energetic calculations were performed at 1 atm pressure and 298.15 K using the Gaussian 16 software.[64] The obtained results were systematically compared to provide consistent insights. In this study, the primary objective is to investigate the effect of coordination-dependent electronic modulation by carborane and silaborane cages on FLP frustration; therefore, only gas-phase calculations were considered. To evaluate the interactions between the Lewis acidic and basic sites, quantum theory of atoms in molecules (QTAIM)[65–67] analyses were conducted using the Multiwfn software package.[68]

To gain further insight into the differing reactivities of the studied IFLPs, the strain developed along the reaction pathway arising from structural distortion of the reactants and the evolution of interaction energies were analyzed. The strain energies in the CMs and TSs were calculated as follows:

$$\Delta E_{\text{strain}}\ (\text{IFLP\_CM}) = E_{\text{IFLP}}^{\text{CM-geom}} - E_{\text{IFLP}}^{\text{opt}}$$

$$\Delta E_{\text{strain}}(\text{CO}_2\text{\_CM}) = E_{\text{CO}_2}^{\text{CM-geom}} - E_{\text{CO}_2}^{\text{opt}}$$

$$\Delta E_{\text{strain}}\ (\text{IFLP\_TS}) = E_{\text{IFLP}}^{\text{TS-geom}} - E_{\text{IFLP}}^{\text{opt or CM-geom}}$$

$$\Delta E_{\text{strain}}(\text{CO}_2\text{\_TS}) = E_{\text{CO}_2}^{\text{TS-geom}} - E_{\text{CO}_2}^{\text{opt(or CM-geom)}}$$

Here, $E^{\text{TS-geom}}$ and $E^{\text{CM-geom}}$ denote the single-point energies of the fragments in the geometries they adopt within the transition state and reactant complex, respectively, while E^{opt} refers to the energy of the fully optimized fragment in its equilibrium structure. The ΔE_{strain} (IFLP_CM), ΔE_{strain} (CO_2_CM) represents the strain induced in the IFLP and CO_2 in the CMs, while ΔE_{strain} (IFLP_TS), ΔE_{strain} (CO_2_TS), indicates the strain induced in the IFLP and CO_2 in the TSs. It is important to note that if a CM is more stable than the isolated reactants, the strain required to reach the TS is referenced from the CM geometries rather than the isolated fragments. The resulting strain–interaction energy profiles provide detailed insights into how different coordinating sites influence the reaction pathways, thereby revealing the impact of coordination dichot-

omy in carborane and silaborane cages on the frustration of the Lewis pairs.

Result & discussion

To obtain an initial estimate of the variation in electronic effects at different coordinating sites of carborane and silaborane, the natural bond orbital (NBO) charges of the cage atoms were calculated. The calculated NBO charges, along with the optimized geometries of *o*-carborane and *o*-silaborane, are provided in Fig. S1 of the SI. Analysis of the NBO charges (Fig. S1) reveals that atoms at the 1st and 2nd positions possess identical charges in both cages. Likewise, the 3rd and 6th, 8th and 10th, 9th and 12th, as well as the 4th, 5th, 7th, and 11th positions exhibit equivalent charges. This similarity in the charges at different coordinating sites indicates that these positions experience comparable electronic effects. Consequently, the electronic dichotomy of the cages can be adequately represented by considering only the 1st, 3rd, 4th, 8th, and 9th positions as unique. To assess how these electronic variations influence the frustration of supported Lewis pairs, the acidity of $-BH_2$ and the basicity of $-PH_2$ substituents were examined at the unique coordinating sites identified above. Acidity and basicity were estimated using hydride ion affinity (HIA) and proton ion affinity (PIA), respectively, as summarized in Table 1. A more negative HIA value corresponds to stronger acidity, while a more negative PIA value corresponds to stronger basicity.

From Table 1, it is evident that moving from the 1st to the 9th coordinating site *via* the 3rd, 4th, and 8th positions, the HIA values become progressively less negative, signifying a decrease in acidity of the $-BH_2$. This trend reflects the gradual increase in electron-donating character at these sites. Correspondingly, the PIA values increase (*i.e.*, becomes more negative), indicating enhanced basicity of the $-PH_2$ unit across the same sequence of positions. Importantly, both *o*-carborane and *o*-silaborane display a similar trend in the variation of acidity and basicity, though the magnitude of these effects differs markedly between the two systems. For example, the HIA of $-BH_2$ at the 1st position in *o*-carborane is −93.96 kcal mol^{-1}, whereas in *o*-silaborane it is significantly more negative (*i.e.*, −120.29 kcal mol^{-1}), highlighting the stronger electron-withdrawing effect of Si relative to C. Further, at the 3rd position, the HIA of $-BH_2$ in *o*-carborane is ∼3 kcal mol^{-1} lower than in *o*-silaborane (see Table 1), indicating that the B atom at 3rd position in *o*-carborane is more electron withdrawing than the corresponding atom in *o*-silaborane. This electronic disparity is also reflected in the PIA values. The $-PH_2$ unit at the 3rd coordinating site in *o*-carborane has a PIA of 2.25 kcal mol^{-1}, compared to −7.14 kcal mol^{-1} in *o*-silaborane, indicating greater basicity in the latter. A similar trend is observed at the 4th, 8th, and 9th coordinating sites, where *o*-carborane consistently shows higher HIA values (more acidic $-BH_2$) compared to *o*-silaborane.

Conversely, *o*-silaborane exhibits significantly more negative PIA values at these sites *i.e.*, −12.60, −20.61, and −22.31 kcal mol^{-1}, respectively, confirming its stronger electron-donating character relative to *o*-carborane. Thus, the comparative analysis of HIA and PIA values demonstrates that while both cages exhibit analogous electronic dichotomy, *o*-silaborane exerts more pronounced electron-withdrawing and electron-donating effects at 1st and 9th coordinating sites in comparison to the *o*-carborane. This distinction underscores the importance of examining how the coordination dichotomy of the silaborane cage influences the frustration of supported Lewis pairs. The distinct electronic behavior of the o-silaborane cage, as reflected in the HIA and PIA trends, is further supported by experimental photoelectron spectroscopic data. Seyferth and co-workers reported He(I) photoelectron spectra for 1,2-disila-*closo*-dodecaborane, which revealed that the silaborane cage possesses a notably more electron-rich valence framework than its carborane counterpart.[57,58] This observation arises from the greater ability of silicon to donate electron density into the delocalized cage bonding network, owing to its lower effective nuclear charge and more diffuse valence orbitals relative to carbon. Consequently, while the cage as a whole becomes more electron rich, the Si atom itself becomes more electron deficient, thereby exerting a stronger inductive electron-withdrawing influence on substituents bound to it. The enhanced acidity of $-BH_2$ and the deeper PIA values observed in *o*-silaborane at several coordinating positions align precisely with this experimental insight. Thus, the He(I) photoelectron spectrum not only validates the intrinsic electronic enrichment of the silaborane cage but also corroborates the stronger inductive modulation exerted by silicon, reinforcing the interpretation of the HIA/PIA trends discussed above.

Table 1 Hydride Ion Affinity (HIA) of $-BH_2$ and Proton Ion Affinity (PIA) of $-PH_2$ at Different Coordinating Sites of Carborane and Silaborane Cages

General structure of the *o*-carborane and *o*-silaborane cage

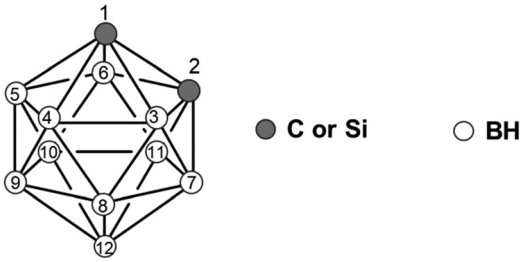

	Hydride ion affinity (kcal mol^{-1})		Proton ion affinity (kcal mol^{-1})	
	$-BH_2 + H^- \rightarrow [BH_3]^-$		$-PH_2 + H^+ \rightarrow [PH_3]^+$	
Coordinating sites	C	Si	C	Si
1st	−93.96	−120.29	16.64	23.02
3rd	−85.76	−82.54	2.25	−7.14
4th	−76.25	−75.41	−5.76	−12.60
8th	−68.53	−66.68	−14.25	−20.61
9th	−65.77	−64.30	−17.15	−22.31

To this end, various unique combinations of adjacent coordinating sites were considered for Lewis pair substitution, as illustrated in Fig. 1d. The coordinating sites for the $-BH_2$ and $-PH_2$ units were selected based on two criteria: (a) the sites must be adjacent, and (b) the electronic effect at these sites should favour either the acidic fragment ($-BH_2$), the basic fragment ($-PH_2$), or both. Initially, $-BH_2$ was placed at the 1st position and $-PH_2$ at the 2nd position, such that the electron-withdrawing effect at the 1st site enhanced the acidity of $-BH_2$ while simultaneously reducing the basicity of $-PH_2$. Subsequently, the $-PH_2$ group was shifted to the 3rd and 4th positions, with $-BH_2$ fixed at the 1st position, to improve the basicity of the $-PH_2$ site. In another arrangement, $-BH_2$ was moved from the 1st to the 4th and 12th positions, corresponding to the relocation of $-PH_2$ to the 9th coordinating site. These substitutions collectively increased the basicity of $-PH_2$ while decreasing the acidity of $-BH_2$. Finally, the groups were positioned with $-BH_2$ at the 3rd site and $-PH_2$ at the 8th site, a configuration expected to impart moderate electronic effects on both acidic and basic centres. The IFLPs generated from these positional variations (see Fig. 1d) were fully optimised and analysed to assess the initial electronic influences of the coordinating sites.

Analysis of Fig. 2 shows that relocating the $-PH_2$ unit from Y2 (Y = C, Si) in ^{Y}PB1 to B3 and B4 in ^{Y}PB2 and ^{Y}PB3 results in a slight but noticeable decrease in the P–B bond distance, accompanied by an increase in the electron density (ρ) at the bond critical point (X) between the P and B atoms. For example, in ^{C}PB1 the P–B distance is 2.09 Å, which shortens to 2.07 Å in ^{C}PB2 and 2.06 Å in ^{C}PB3. Correspondingly, the electron density (ρ) at X increases from 0.0805 a.u. in ^{C}PB1 to 0.0875 and 0.0904 a.u. in ^{C}PB2 and ^{C}PB3, respectively. A similar trend in P–B distances and electron densities can be observed for the ^{Si}PBn (n = 1–3) systems. These observations indicate stronger P–B interactions upon relocating the $-PH_2$ group to the B3 and B4 sites, consistent with the enhanced basicity of the $-PH_2$ substituent at these positions, as reflected in the PIA values (see Table 1). It is further evident from Fig. 2 that silaborane-supported IFLPs exhibit shorter P–B distances and higher electron densities at X compared to their carborane-supported counterparts. For instance, the PB distance in ^{Si}PB1 was observed to be 2.02 Å which is 0.07 Å smaller than the PB distance in ^{C}PB1, also the ρ at Y in ^{Si}PB1 was found to be 0.0951 a. u. which is greater than in case of ^{C}PB1. Similar observation can also be made for ^{Si}PB2 and ^{Si}PB3 from Fig. 2. These observations can be attributed to the more pronounced electron-withdrawing and electron-donating effects at the 1st–4th positions of the silaborane cage relative to the carborane cage, as indicated by the HIA and PIA values discussed earlier.

Fig. 3 shows that in ^{C}PB4 and ^{Si}PB4, relocation of the $-BH_2$ group from Y1 (Y = C, Si) to the B4 position, along with the corresponding shift of the $-PH_2$ group to B9, leads to a decrease in electron density (ρ) at the X and an increase in the P–B distance relative to ^{Y}PB3 (Y = C, Si). The repositioning of $-PH_2$ to B9 enhances its basicity, as indicated by the PIA values (see Table 1). However, the transfer of $-BH_2$ from C1/Si1 to B4 reduces its acidity, thereby diminishing its electron-accepting ability. This combination results in the elongation of the P–B bond and the reduction of ρ. Further relocation of $-BH_2$ and $-PH_2$ from B4 to B9 and from B9 to B12, respectively, forming ^{C}PB5, produces an additional increase in P–B distance and a further decrease in ρ. An even more pronounced effect is observed in ^{Si}PB5, which exhibits the longest P–B distance (3.57 Å) and the absence of a bond critical point between P and B atoms among all the IFLPs studied so far. This striking behaviour can be attributed to the strongly quenched acidity of the $-BH_2$ group at the B4 position in ^{Si}PB5 compared to other cases. Finally, placement of the $-BH_2$ and $-PH_2$ groups at the second most electron-withdrawing and electron-donating positions, namely the 3rd and 8th sites of the cages, generates the IFLPs ^{C}PB6 and ^{Si}PB6. These systems exhibit moderate P–B bond distances of 2.07 and 2.04 Å and ρ of 0.0886 and 0.0913 a.u., respectively. Overall, the electronic structure analysis of the IFLPs provides an initial understanding of how coordination dichotomy influences the reactivity of the active site.

It also highlights differences in the extent of electronic effects between carborane and silaborane cages, consistent with the acidity and basicity trends reflected in the HIA and PIA values. The optimized geometries of the CMs formed through the interaction of CO_2 with silaborane- and carborane-based IFLPs are depicted in Fig. 4 and Fig. S2 (SI), along with the zero-point corrected relative energies (ΔE, in kcal mol^{-1}) and the key geometrical parameters. From the optimized structures shown in Fig. 4 and S2, it is evident that CO_2 binding induces expansion of the P–B bond and an increase in the angle projected by the $-PH_2$ and $-BH_2$ groups on the silaborane and carborane cages. This structural distortion suggests that CO_2 coordination introduces strain into the molecular system, which in turn governs the overall relative energies of the resulting CMs. Accordingly, strain–interaction profiles have been calculated and are presented in Fig. 4 and S2. For silaborane, in ^{Si}PB1$_{CM}$ the P–C and B–O distances and O–C–O bond angle were 3.92 Å, 2.39 Å, and 178.9°, respectively (see Fig. 4). The calculated interaction energy was −6.32 kcal mol^{-1}, while the strain energy was 1.80 kcal mol^{-1}. Since the interaction energy dominates the induced strain, a stable CM (^{Si}PB1$_{CM}$) is formed, with ΔE = −5.26 kcal mol^{-1}. In ^{Si}PB2$_{CM}$, the P–C and B–O distances and O–C–O angle were 3.44 Å, 2.06 Å, and 176.8°, respectively, which are smaller than in ^{Si}PB1$_{CM}$. This contraction indicates stronger interaction between CO_2 and the IFLP ^{Si}PB2, consistent with the enhanced basicity of the $-PH_2$ group as suggested earlier by PIA values. The interaction energy was −9.92 kcal mol^{-1}, more negative than in ^{Si}PB1$_{CM}$. However, the strain developed in ^{Si}PB2$_{CM}$ was nearly 20 kcal mol^{-1} greater than in ^{Si}PB1$_{CM}$ (Fig. 4). Similarly, in ^{Si}PB3$_{CM}$ the P–C and B–O distances and the O–C–O angle decreased further, reflecting enhanced interaction, as supported by the calculated interaction energy of −11.89 kcal mol^{-1} (see Fig. 4).

In this case, however, the induced strain reached 28.58 kcal mol^{-1}, higher than in ^{Si}PB2$_{CM}$. For both ^{Si}PB2$_{CM}$ and ^{Si}PB3$_{CM}$, the strain energy dominates the interaction energy, resulting in relatively unstable CMs with ΔE values of 11.02 kcal mol^{-1}

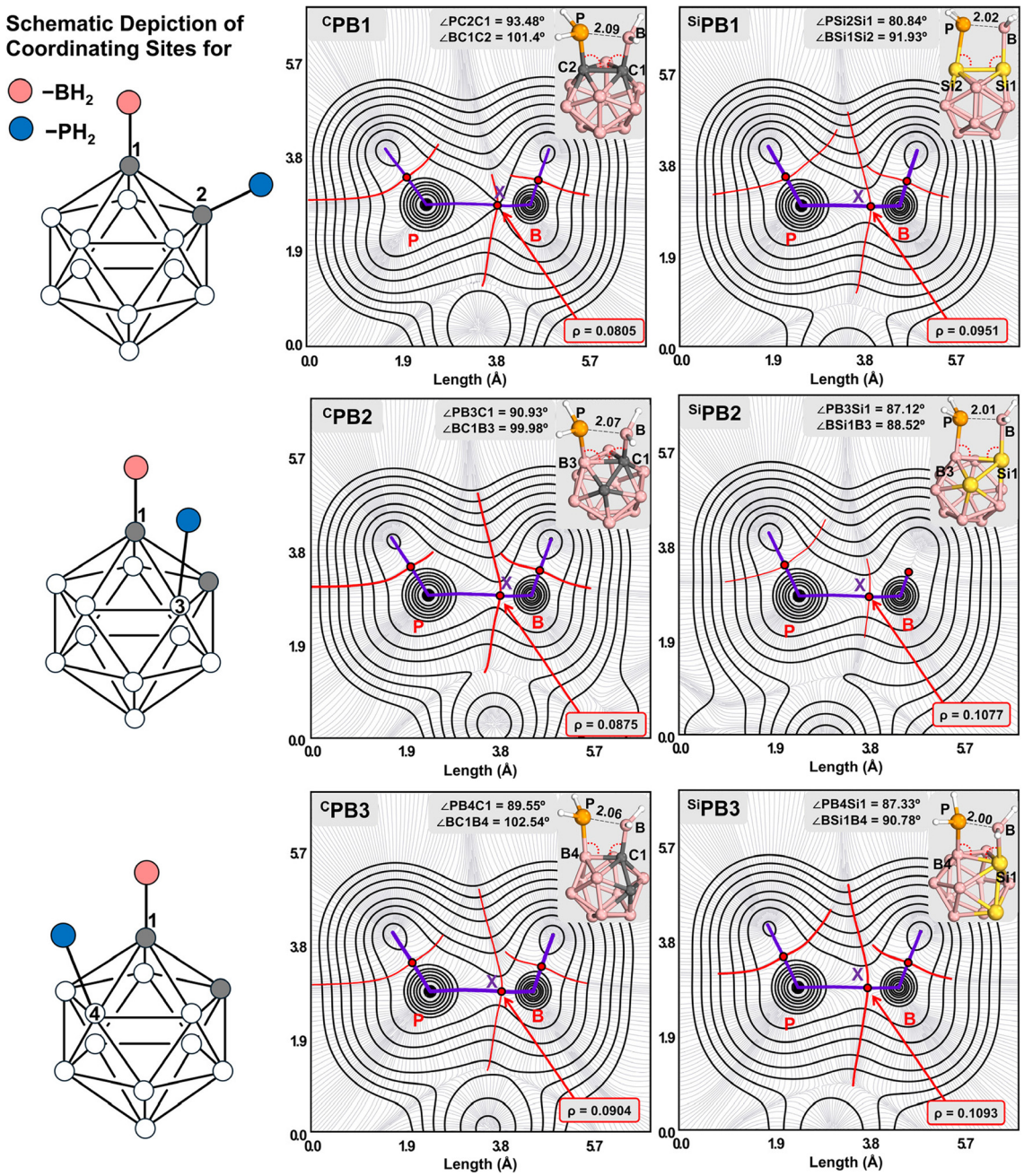

Fig. 2 Electron density contour plots along with optimized geometries of ^{Y}PBn (Y = C, Si and n = 1–3) IFLPs. (The distances are in angstrom, red solid circles in the electron density plots represents bond critical point (BCP) X, electron density (ρ) is in a.u., electron density was plotted at 0.001 a. u. iso value).

and 16.34 kcal mol^{-1}, respectively. It is noteworthy that the induced strain correlates with the extent of intramolecular –PH$_2$···–BH$_2$ interaction in ^{Si}PB1, ^{Si}PB2, and ^{Si}PB3, as indicated by the ρ values at the bond critical point (X). The order of strain energies (*i.e.*, ^{Si}PB1$_{CM}$ < ^{Si}PB2$_{CM}$ < ^{Si}PB3$_{CM}$) follows the trend in ρ values (*i.e.*, ^{Si}PB1 < ^{Si}PB2 < ^{Si}PB3). Thus, higher ρ values imply stronger internal interactions, requiring proportionally higher energies to achieve the geometrical deformations necessary for CO_2 binding. Further, in ^{Si}PB4$_{CM}$, the interaction energy was −5.64 kcal mol^{-1} which is less negative than in ^{Si}PB3$_{CM}$, while the induced strain was 5.81 kcal mol^{-1}, nearly 23 kcal mol^{-1} lower than in ^{Si}PB3$_{CM}$. The reduced interaction energy arises from diminished acidity of the –BH$_2$ group, consistent with longer B–O and P–C distances and a larger O–C–O angle compared to ^{Si}PB3$_{CM}$. The smaller strain is attributed to weaker –PH$_2$···–BH$_2$ interaction, as reflected in the lower ρ value.

Furthermore, in ^{Si}PB5$_{CM}$, the induced strain was only 0.36 kcal mol^{-1}, the smallest among all investigated systems. The absence of BCP (X) confirms negligible interaction

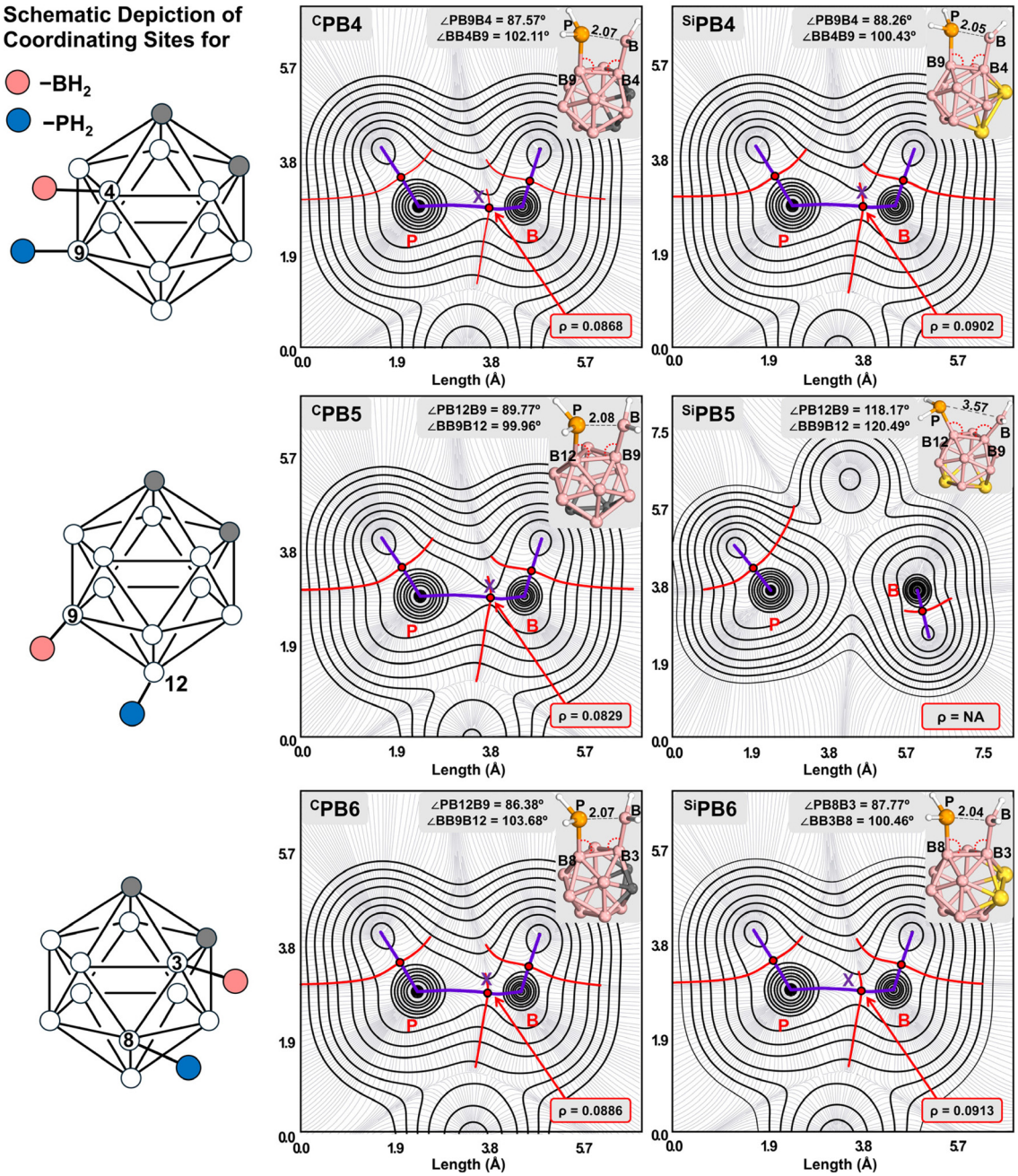

Fig. 3 Electron density contour plots along with optimized geometries of ^{Y}PBn (Y = C, Si and n = 4–6) IFLPs. (The distances are in angstrom, red solid circles in the electron density plots represents bond critical point (BCP) X, electron density (ρ) is in a.u., electron density was plotted at 0.001 a. u. iso value).

between –PH_2 and –BH_2 units, justifying the minimal energy required to deform the structure for CO_2 binding. The interaction energy was −4.95 kcal mol^{-1} which is less negative than in $^{Si}PB4_{CM}$, reflecting further reduced –BH_2 acidity, as indicated by the longer P–C and B–O distances and the wider O–C–O angle. In both $^{Si}PB4_{CM}$ and $^{Si}PB5_{CM}$, the interaction energy governs stability due to the low induced strain, yielding ΔE values of −0.39 and −3.70 kcal mol^{-1}, respectively. In $^{Si}PB6_{CM}$, the strain energy was 8.28 kcal mol^{-1}, higher than in $^{Si}PB4_{CM}$ and $^{Si}PB5_{CM}$. This increase is attributed to the larger ρ value at BCP (X), indicating stronger –PH_2···–BH_2 interaction. The interaction energy was −5.68 kcal mol^{-1}, more negative than in $^{Si}PB5_{CM}$, consistent with shorter P–C (3.47 Å) and B–O (2.48 Å) distances and a reduced O–C–O angle of 177.6°. In this case, strain dominates over the stabilizing interaction, producing a relatively unstable CM ($^{Si}PB6_{CM}$) with ΔE = 1.92 kcal mol^{-1}.

Like in the case of $^{Si}PB1$, the interaction of CO_2 with $^{C}PB1$ results in the formation of a CM (*i.e.*, $^{C}PB1_{CM}$) with a ΔE value

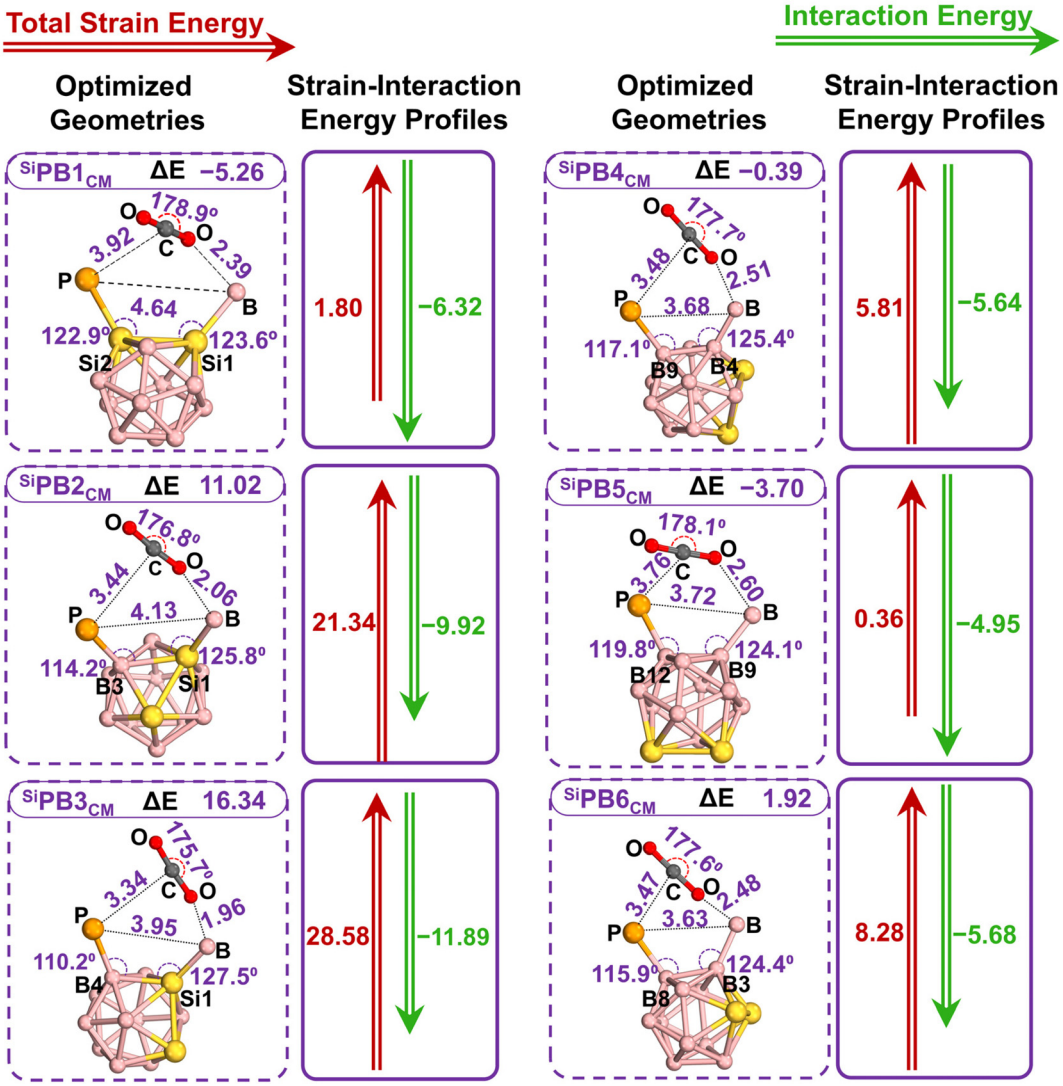

Fig. 4 Optimized geometries of the reactant complexes (CMs) formed by the interaction of CO_2 with silaborane supported IFLPs along with corresponding strain and interaction profiles. (The distances are in angstroms, ΔE is the zero-point corrected relative energy in kcal mol^{-1}, the number in red in the strain-interaction profile represents the strain induced (in kcal mol^{-1}) while the number in green shows the interaction energy (in kcal mol^{-1}) between CO_2 and the IFLP).

of −4.35 kcal mol^{-1} (see Fig. S2 in SI). The dominance of the interaction energy (−4.33 kcal mol^{-1}) over the minute strain (0.21 kcal mol^{-1}) developed in the structure accounts for the observed stability of $^{C}PB1_{CM}$. However, both the strain and interaction energies are smaller than those in $^{Si}PB1_{CM}$, thereby justifying the comparatively lower stability of $^{C}PB1_{CM}$ with respect to $^{Si}PB1_{CM}$. In $^{C}PB2_{CM}$, a higher strain of 8.67 kcal mol^{-1} is induced upon interaction with CO_2, while the calculated interaction energy amounts to −5.98 kcal mol^{-1} (Fig. S2). The strain developed in $^{C}PB2_{CM}$ is significantly smaller than in its silaborane-supported analogue, $^{Si}PB2_{CM}$. This lower strain explains the reduced ΔE value of 2.29 kcal mol^{-1} for $^{C}PB2_{CM}$ compared to $^{Si}PB2_{CM}$ (Fig. S2). Unlike $^{Si}PB3_{CM}$, where both strain and interaction energies are larger than those in $^{Si}PB2_{CM}$ due to the enhanced basicity, $^{C}PB3_{CM}$ exhibits lower strain and interaction energies, with values of 5.41 kcal mol^{-1} and −5.27 kcal mol^{-1}, respectively (see Fig. S2), both smaller than in $^{C}PB2_{CM}$ despite the enhanced basicity of the –PH_2 unit in $^{C}PB3_{CM}$.

To rationalise this apparent inconsistency, the electronic structures of the optimised geometries of $^{C}PB2_{CM}$ and $^{C}PB3_{CM}$ were critically analysed. It can be seen form Fig. 5 that in $^{C}PB2_{CM}$, the oxygen atom of CO_2 interacts with the acidic hydrogen at C2. The ρ value at the corresponding BCP was measured to be 0.08812 a.u. In $^{C}PB3_{CM}$, however, the O atom interacts with the H at B3, yielding a ρ value of 0.06688 a.u., which is smaller than in $^{C}PB2_{CM}$, signifying a weaker interaction in $^{C}PB3_{CM}$. This variation is further supported by the O–H distances, which are 2.72 Å in $^{C}PB3_{CM}$ compared to the shorter O–H distance observed in $^{C}PB2_{CM}$ (Fig. 5). The inter-

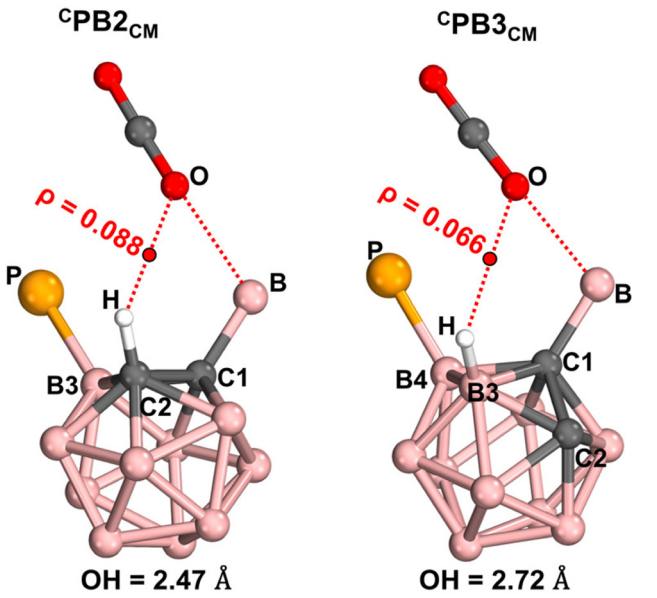

Fig. 5 Optimized geometries of $^{C}PB2_{CM}$ and $^{C}PB3_{CM}$ signifying the interaction with the H atom at C2 and B3, respectively. (ρ is in a.u.).

action with the acidic hydrogen at C2 thus leads to slightly stronger interaction in $^{C}PB2_{CM}$. Consequently, the weaker interaction in $^{C}PB3_{CM}$ induces smaller structural distortion, leading to reduced strain relative to $^{C}PB2_{CM}$ and thereby justifying the higher stability of $^{C}PB3_{CM}$ over $^{C}PB2_{CM}$.

In $^{C}PB4_{CM}$ and $^{C}PB5_{CM}$, both strain energies and interaction energies decrease due to the reduced acidity of the $-BH_2$ unit and diminished interaction between the $-PH_2$ and $-BH_2$ groups. In these cases, the dominance of interaction energy over induced strain results in CMs with negative ΔE values (see Fig. S2), confirming their stability. Finally, in $^{C}PB6_{CM}$, the strain and interaction energies are 3.32 kcal mol^{-1} and −6.04 kcal mol^{-1}, respectively, both greater than those observed in $^{C}PB4_{CM}$ and $^{C}PB5_{CM}$ (Fig. S2). This increase arises from the higher acidity of the $-BH_2$ group and the stronger interaction between the $-BH_2$ and $-PH_2$ units, as indicated by the ρ value at X in $^{C}PB6_{CM}$ (see Fig. 3). Overall, this analysis provides insight into how the coordination of the Lewis acid (LA) and Lewis base (LB) over the cages influences their mode of interaction with the CO_2 molecule. These variations result in CMs with distinct energy profiles, which may in turn affect the course of the reaction.

To further investigate the activity, *i.e.*, the extent of frustration, the transition states (TSs) along with their geometrical parameters, ΔE, and activation energies (E_a) were evaluated and are presented in Fig. 6, along with their corresponding strain–interaction energy profiles. It can be clearly seen from Fig. 6 that, in attaining the TS geometries from the reactant complexes, the P–B and B–O distances, the OCO bond angle, and the angles projected by the $-PH_2$ and $-BH_2$ groups on the cage become shorter than the corresponding parameters in the CMs. This signifies the increased interaction between CO_2 and the IFLPs, as well as the enhanced strain in the molecular system. The E_a for $^{C}PB1_{TS}$ was calculated to be 14.19 kcal mol^{-1}, while the strain and interaction energies were found to be 38.20 and −29.31 kcal mol^{-1}, respectively, in going from $^{C}PB1_{CM}$ to $^{C}PB1_{TS}$. In contrast, $^{Si}PB1_{TS}$ exhibited strain energy nearly 10 kcal mol^{-1} higher than $^{C}PB1_{TS}$, which accounts for its higher E_a of 18.97 kcal mol^{-1}, despite having stronger interaction than $^{C}PB1_{TS}$. Further, in going from $^{C}PB1_{TS}$ to $^{C}PB2_{TS}$, the induced strain was reduced by ∼3 kcal mol^{-1}, accompanied by a slight decrease of nearly 1 kcal mol^{-1} in the interaction energy. The diminished strain in $^{C}PB2_{TS}$ results in a lower E_a of 11.37 kcal mol^{-1} compared to $^{C}PB1_{TS}$. Likewise, in $^{Si}PB2_{TS}$ the strain was ∼5 kcal mol^{-1} smaller than in $^{Si}PB1_{TS}$, justifying the smaller E_a of 15.33 kcal mol^{-1}. However, this value still remains higher than the E_a of $^{C}PB2_{TS}$ due to the greater strain in $^{Si}PB2_{TS}$. In the case of $^{C}PB3$, the strain induced in achieving the TS geometry from $^{C}PB3_{CM}$ was found to be 25.6 kcal mol^{-1}, while the interaction energy was −18.79 kcal mol^{-1}. The relatively lower strain developed in $^{C}PB3_{TS}$ results in a reduced E_a of 7.79 kcal mol^{-1} compared to $^{C}PB2_{TS}$. Furthermore, the induced strain energies in $^{C}PB4_{TS}$, $^{C}PB5_{TS}$, and $^{C}PB6_{TS}$ were observed to be 28.96, 31.16, and 27.32 kcal mol^{-1}, respectively, with interaction energies of approximately −18.5 kcal mol^{-1} in all cases.

Consequently, the E_a values for $^{C}PB4_{TS}$, $^{C}PB5_{TS}$, and $^{C}PB6_{TS}$ were 11.10, 13.19, and 9.06 kcal mol^{-1}, respectively, following the same order as the induced strain. Having nearly identical interaction energies, the activation barriers in these cases are controlled primarily by the strain induced in the structures. Unlike $^{C}PB3_{TS}$, $^{Si}PB3_{TS}$ exhibits a strain energy of 44.15 kcal mol^{-1}, which is considerably higher than that in $^{Si}PB2_{TS}$, resulting in an E_a of 18.67 kcal mol^{-1}, greater than that of $^{Si}PB2_{TS}$. In the subsequent case of $^{Si}PB4_{TS}$, the E_a was found to be nearly half of that in $^{Si}PB3_{TS}$. This decrease can be attributed to the lower strain energy of 24.64 kcal mol^{-1} in $^{Si}PB4_{TS}$, which is also approximately half of that in $^{Si}PB3_{TS}$. It is noteworthy that $^{Si}PB4_{TS}$ has a lower E_a than its carborane-based analogue, $^{C}PB4_{TS}$, again due to smaller induced strain in the former (see Fig. 6). For $^{Si}PB5_{TS}$, the induced strain was 29.53 kcal mol^{-1}, greater than in $^{Si}PB4_{TS}$, leading to an E_a of 12.89 kcal mol^{-1}, which is higher than in $^{Si}PB4_{TS}$. Interestingly, $^{Si}PB6_{TS}$ displayed a strain energy of 31.95 kcal mol^{-1}, greater than in $^{Si}PB5_{TS}$. Despite this higher strain, the calculated E_a was 10.33 kcal mol^{-1}, which is lower than in $^{Si}PB5_{TS}$ (see Fig. 6). This reduced barrier can be attributed to the stronger interaction in $^{Si}PB6_{TS}$, reflected in the more negative interaction energy of −21.82 kcal mol^{-1} compared to $^{Si}PB5_{TS}$. The overall energetic analysis, based on the strain and interaction energies developed in achieving the TS states *via* the CMs, provides a clear understanding of how the positions of the LA and LB units affect the overall energetics of the reaction. Different coordinating sites not only modulate the acidity and basicity of the active centers but also influence the structural deformations that dictate the reaction profile.

To finally conclude the effect of coordination dichotomy, the relative stabilities of the CO_2 adducts were calculated. The

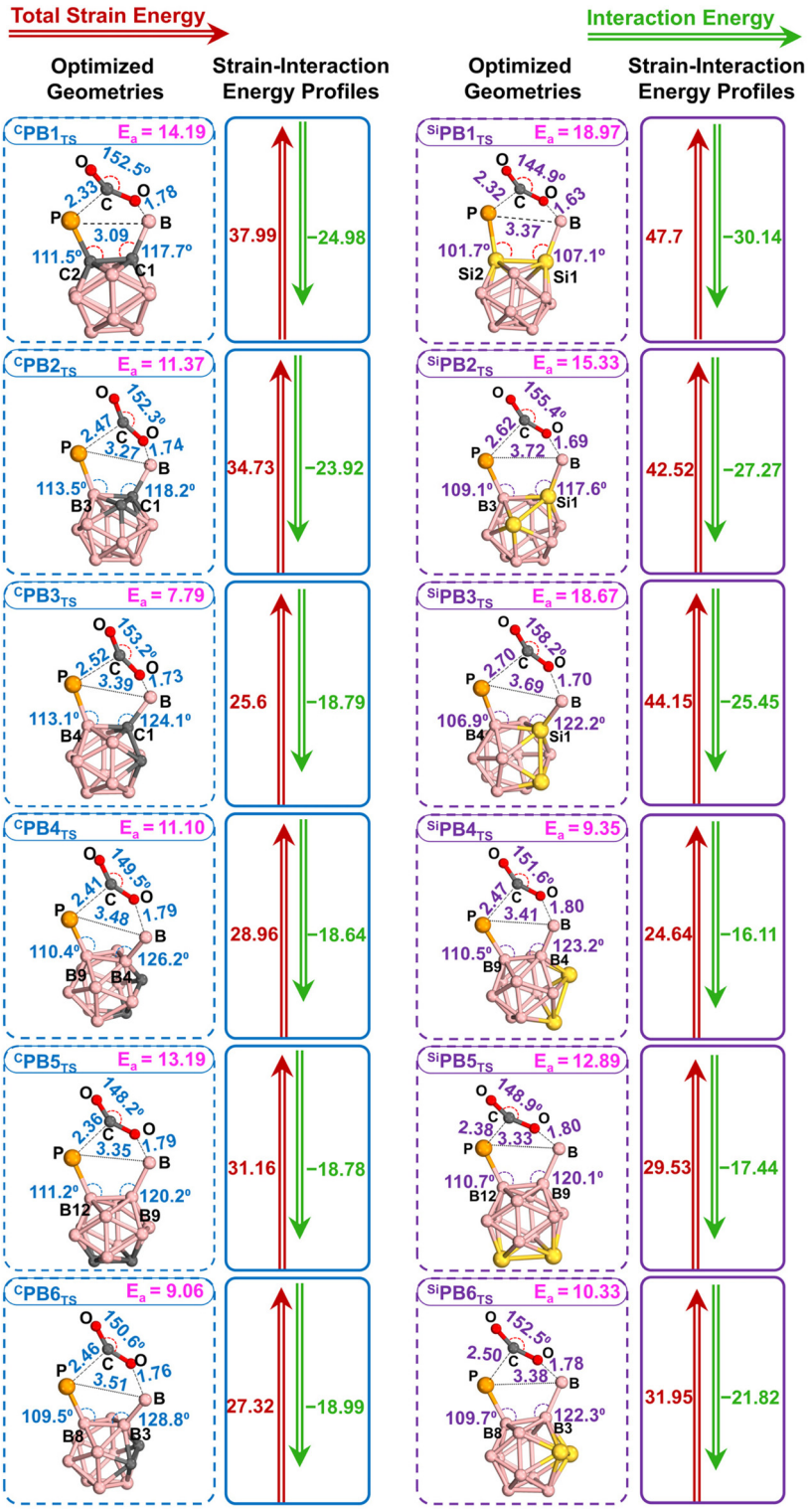

Fig. 6 Optimized geometries of the transition states (TSs) formed in the reaction of CO_2 with silaborane and carborane supported IFLPs along with corresponding strain and interaction profiles. (the distances are in angstroms, E_a is the CO_2 activation energy in kcal mol^{-1}, the number in red in the strain-interaction profile represents the strain induced (in kcal mol^{-1}) while the number in green shows the interaction energy (in kcal mol^{-1}) between CO_2 and the IFLP).

optimized geometries of the formed CO_2 adducts (ADs) with carborane and silaborane IFLPs are shown in Fig. 7, along with the geometrical parameters and the corresponding strain–interaction energy profiles. The zero-point corrected relative energies of the adducts are also given in the Figure. It is evident from the comparative analysis of the geometrical

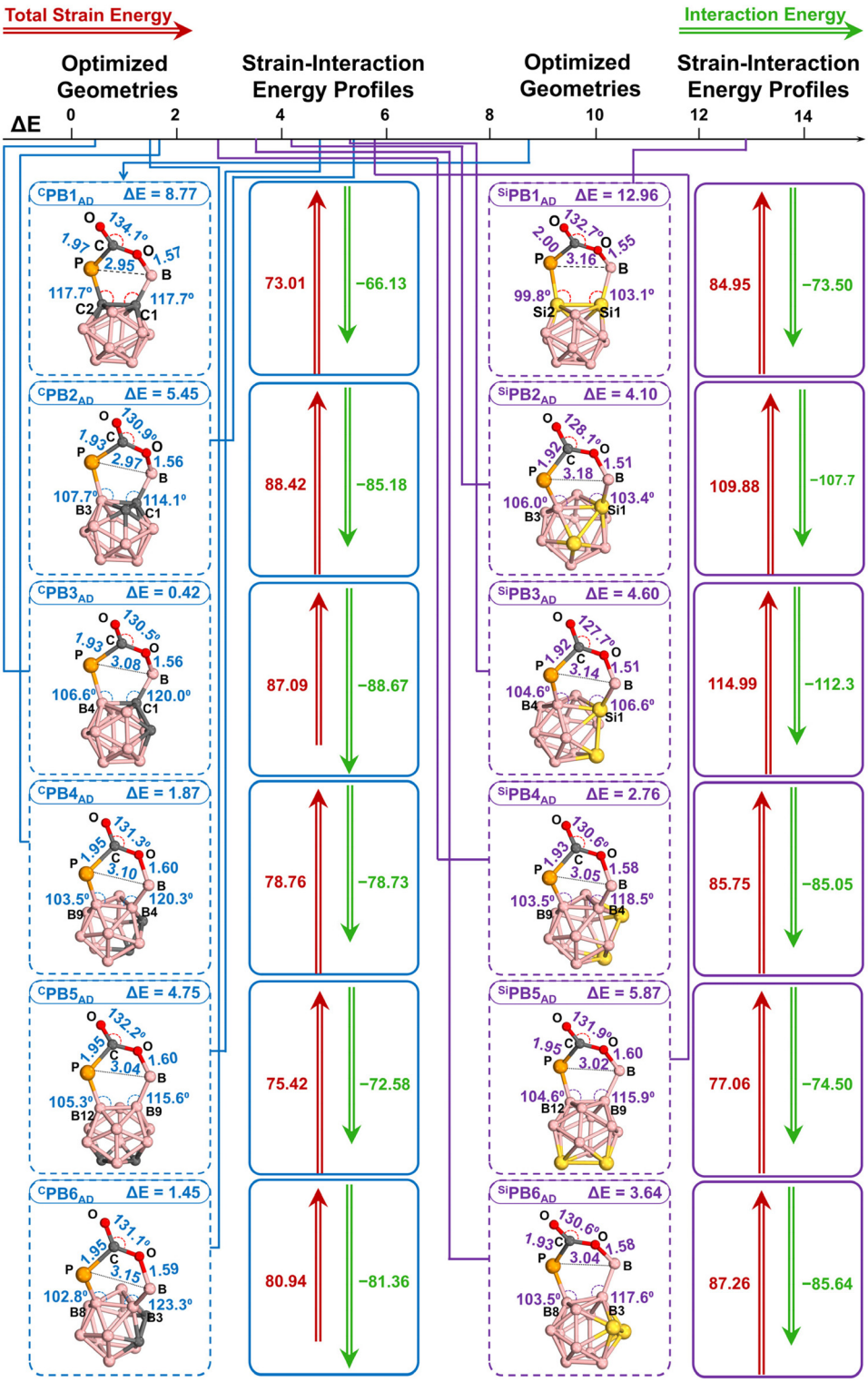

Fig. 7 Optimized geometries of the CO_2 adducts (ADs) formed in the reaction of CO_2 with silaborane and carborane supported IFLPs along with corresponding strain and interaction profiles. (the distances are in angstroms, zero point corrected energies are given in kcal mol^{-1}, the number in red in the strain-interaction profile represents the strain induced (in kcal mol^{-1}) while the number in green shows the interaction energy (in kcal mol^{-1}) between CO_2 and the IFLP).

parameters of CMs, TSs and ADs presented in Fig. 4, 6 and 7 that the CO_2 adducts possess the smallest geometrical parameters, indicating the strongest interaction between CO_2 and the IFLPs and the highest strain developed in the molecular structures. It can be seen in Fig. 7 that the ΔE for $^{C}PB1_{AD}$ is 8.77 kcal mol^{-1}, while for $^{C}PB2_{AD}$ and $^{C}PB3_{AD}$ the values are

5.45 and 0.42 kcal mol^{-1}, respectively. This clearly shows that the relative energy decreases when the –PH_2 group is shifted from C2 to B3 and C4 due to the enhanced basicity of the –PH_2 and thereby strengthens the interaction with CO_2. This enhancement is also reflected in the interaction energies calculated for $^{C}PB1_{AD}$, $^{C}PB2_{AD}$, and $^{C}PB3_{AD}$, which are −66.13, −85.18, and −88.67 kcal mol^{-1}, respectively.

Notably, the strain induced in $^{C}PB2_{AD}$ and $^{C}PB3_{AD}$ (88.42 and 87.09 kcal mol^{-1}) is higher than in $^{C}PB1_{AD}$ (73.01 kcal mol^{-1}) (see Fig. 7), but the stronger interactions stabilize these adducts. In $^{C}PB4_{AD}$, ΔE increases to 1.87 kcal mol^{-1}, higher than in $^{C}PB3_{AD}$, which can be attributed to the reduced interaction energy (−78.73 kcal mol^{-1}). Similarly, $^{C}PB5_{AD}$ exhibits a ΔE of 4.75 kcal mol^{-1} which is greater than $^{C}PB4_{AD}$, again due to a further decrease in interaction energy. Finally, $^{C}PB6_{AD}$, with a ΔE of 1.45 kcal mol^{-1} was found to be more stable than $^{C}PB5_{AD}$ owing to enhanced interaction energy, despite the higher strain observed (Fig. 7). From the ΔE values in Fig. 7, it is also clear that all silaborane-supported CO_2 adducts are less stable than their carborane counterparts except $^{Si}PB2_{AD}$, as their ΔE values are consistently higher. The stability pattern observed in $^{C}PB1_{AD}$ to $^{C}PB2_{AD}$ is reflected in $^{Si}PB1_{AD}$ to $^{Si}PB2_{AD}$. Specifically, the ΔE values decrease from 12.96 to 4.10 kcal mol^{-1}, which can be explained by the significant increase in interaction energy from −73.50 to −107.70 kcal mol^{-1}, despite higher strain. In contrast, $^{Si}PB3_{AD}$ shows a 0.50 kcal mol^{-1} increase in ΔE due to the rise in strain energy from 109.88 to 114.99 kcal mol^{-1}.

Interestingly, $^{Si}PB4_{AD}$ is relatively the most stable among silaborane adducts, with a ΔE of 2.76 kcal mol^{-1}, owing to its much lower strain energy (85.75 kcal mol^{-1}) compared to $^{Si}PB3_{AD}$ (Fig. 7). For $^{Si}PB5_{AD}$ and $^{Si}PB6_{AD}$, the ΔE values are 5.87 and 3.64 kcal mol^{-1}, respectively, following a similar trend to their carborane analogues. Thus, the analysis of adducts provides a comprehensive understanding of how the coordination dichotomy in carborane and silaborane frameworks influences the stability of the formed CO_2 adducts. Overall, silaborane-based IFLPs show their lowest activation barrier and most stable CO_2 adduct in $^{Si}PB4$, while among the *o*-carborane-supported IFLPs, $^{C}PB3$ exhibits both the lowest activation barrier and the most stable adduct. This highlights the distinct electronic effects of carborane and silaborane cages on the LA–LB pair, which ultimately dictate their reactivity.

Additional analyses were carried out to assess the influence of more realistic substituents and alternative small-molecule activation pathways. Substituted IFLPs incorporating –PH_2/B$(CF_3)_2$ and –PMe_2/B$(CF_3)_2$ pairs were examined at the most reactive coordination sites ($^{C}PB3$ for *o*-carborane and $^{Si}PB4$ for *o*-silaborane). The computed CO_2 activation barriers for these substituted systems remain comparable to those of the corresponding unsubstituted IFLPs, consistent with the idea that the intrinsic cage-induced electronic effects dominate the reactivity trends. Furthermore, to determine whether the observed patterns are general beyond CO_2 activation, H_2 activation was also investigated across the same series. Both substrates follow parallel trends in CM energies, activation barriers, and adduct stabilities, with $^{C}PB3$ emerging as the most effective scaffold in each case. These results collectively confirm that the conclusions drawn from CO_2 activation are robust and extend across different substituents and activation pathways. Full computational details, comparative energetics, and optimized structures are provided in the SI.

Conclusion

In presented work, the coordination-dependent electronic effects of the *o*-silaborane cage were introduced and systematically compared with those of *o*-carborane in governing the frustration of intramolecular Lewis pairs (IFLPs). Our analysis demonstrates that silaborane exerts a stronger electronic influence than carborane, in both its electron-withdrawing and electron-donating capacities, with this influence manifesting differently in modulating dichotomy and frustration. The results reveal that the reactivity of silaborane- and carborane-based IFLPs toward CO_2 differs markedly in terms of interaction energies, stability, and strain distribution, all of which are strongly dependent on the positional arrangement of the Lewis acid (LA) and Lewis base (LB) sites within the cages. Transition-state analysis further highlighted distinct activation barriers for the two systems, underscoring their contrasting activities in CO_2 activation. Among the carborane-supported IFLPs, $^{C}PB3$ was identified as the most reactive, with –BH_2 at the 1st position (maximum acidity) and –PH_2 at the 4th position (moderate basicity). In contrast, silaborane displayed its lowest activation barrier in $^{Si}PB4$, where –BH_2 at the 4th position (moderate acidity) and –PH_2 at the 9th position (maximum basicity) provided the optimal combination. This comparison highlights a fundamental distinction that CO_2 activation in carborane systems is governed primarily by the acidity of the –BH_2 unit, whereas silaborane systems are dominated by the basicity of the –PH_2 unit.

Overall, this study establishes silaborane as a promising and stable bridging scaffold for tuning the frustration of Lewis pairs, offering electronic control distinct from that of carborane. These insights pave the way for the rational design of next-generation metal-free catalysts for CO_2 activation and other small-molecule transformations.

Conflicts of interest

The authors declare no competing financial interests.

Data availability

The data supports the findings is provided in the manuscript and the supplementary information (SI). Supplementary information: NBO charges of atoms in carborane and silaborane cages, optimized geometries of the reactant complexes found in the reaction of CO_2 with carborane supported IFLPs are

given in the SI. The cartesian coordinates of the optimized structures are also provided. See DOI: https://doi.org/10.1039/d5dt02382c.

Acknowledgements

This work is supported by SERB (EEQ/2023/000424, EEQ/2019/000656 and ECR/2018/002346). With due respect and sense of obligation we would like to thank NIT Warangal for providing necessary facilities during the research work. The authors M. F. is thankful to the Ministry of Education (MoE), formerly the Ministry of Human Resource Development (MHRD) for providing Senior Research Fellowship (SRF).

References

1 G. C. Welch, R. R. S. Juan, J. D. Masuda and D. W. Stephan, Reversible, Metal-Free Hydrogen Activation, *Science*, 2006, **314**, 1124–1126.
2 G. Ménard and D. W. Stephan, Room Temperature Reduction of CO_2 to Methanol by Al-Based Frustrated Lewis Pairs and Ammonia Borane, *J. Am. Chem. Soc.*, 2010, **132**, 1796–1797.
3 F.-G. Fontaine, M.-A. Courtemanche and M.-A. Légaré, Transition-Metal-Free Catalytic Reduction of Carbon Dioxide, *Chem. – Eur. J.*, 2014, **20**, 2990–2996.
4 C. M. Mömming, E. Otten, G. Kehr, R. Fröhlich, S. Grimme, D. W. Stephan and G. Erker, Reversible Metal-Free Carbon Dioxide Binding by Frustrated Lewis Pairs, *Angew. Chem., Int. Ed.*, 2009, **48**, 6643–6646.
5 E. Theuergarten, T. Bannenberg, M. D. Walter, D. Holschumacher, M. Freytag, C. G. Daniliuc, P. G. Jones and M. Tamm, Computational and experimental investigations of CO_2 and N_2O fixation by sterically demanding N-heterocyclic carbenes (NHC) and NHC/borane FLP systems, *Dalton Trans.*, 2014, **43**, 1651–1662.
6 G. Ménard, T. M. Gilbert, J. A. Hatnean, A. Kraft, I. Krossing and D. W. Stephan, Stoichiometric Reduction of CO_2 to CO by Phosphine/AlX_3-Based Frustrated Lewis Pairs, *Organometallics*, 2013, **32**, 4416–4422.
7 A. L. Travis, S. C. Binding, H. Zaher, T. A. Q. Arnold, J.-C. Buffet and D. O'Hare, Small molecule activation by frustrated Lewis pairs, *Dalton Trans.*, 2013, **42**, 2431–2437.
8 C. Appelt, H. Westenberg, F. Bertini, A. W. Ehlers, J. C. Slootweg, K. Lammertsma and W. Uhl, Geminal Phosphorus/Aluminum-Based Frustrated Lewis Pairs: C–H versus C≡C Activation and CO_2 Fixation, *Angew. Chem., Int. Ed.*, 2011, **50**, 3925–3928.
9 F. Bertini, V. Lyaskovskyy, B. J. J. Timmer, F. J. J. de Kanter, M. Lutz, A. W. Ehlers, J. C. Slootweg and K. Lammertsma, Preorganized Frustrated Lewis Pairs, *J. Am. Chem. Soc.*, 2012, **134**, 201–204.
10 C. Das Neves Gomes, E. Blondiaux, P. Thuéry and T. Cantat, Metal-Free Reduction of CO_2 with Hydroboranes: Two Efficient Pathways at Play for the Reduction of CO_2 to Methanol, *Chem. – Eur. J.*, 2014, **20**, 7098–7106.
11 B. R. Barnett, C. E. Moore, A. L. Rheingold and J. S. Figueroa, Frustrated Lewis pair behavior of monomeric (boryl)iminomethanes accessed from isocyanide 1,1-hydroboration, *Chem. Commun.*, 2015, **51**, 541–544.
12 M. Ferrer, I. Alkorta, J. Elguero and J. M. Oliva-Enrich, Sequestration of Carbon Dioxide with Frustrated Lewis Pairs Based on N-Heterocycles with Silane/Germane Groups, *J. Phys. Chem. A*, 2021, **125**, 6976–6984.
13 J. J. Chi, T. C. Johnstone, D. Voicu, P. Mehlmann, F. Dielmann, E. Kumacheva and D. W. Stephan, Quantifying the efficiency of CO_2 capture by Lewis pairs, *Chem. Sci.*, 2017, **8**, 3270–3275.
14 S. Maeda and K. Ohno, No activation barrier synthetic route of glycine from simple molecules (NH_3, CH_2, and CO_2) via carboxylation of ammonium ylide: a theoretical study by the scaled hypersphere search method, *Chem. Phys. Lett.*, 2004, **398**, 240–244.
15 Y. Kayaki, M. Yamamoto and T. Ikariya, N-Heterocyclic Carbenes as Efficient Organocatalysts for CO_2 Fixation Reactions, *Angew. Chem., Int. Ed.*, 2009, **48**, 4194–4197.
16 J. Baltrusaitis, E. V. Patterson and C. Hatch, Computational Studies of CO_2 Activation via Photochemical Reactions with Reduced Sulfur Compounds, *J. Phys. Chem. A*, 2012, **116**, 9331–9339.
17 I. Alkorta, C. Trujillo, G. Sánchez-Sanz and J. Elguero, Solvent and Substituent Effects on the Phosphine + CO_2 Reaction, *Inorganics*, 2018, **6**, 110.
18 D. Zhuang, A. M. Rouf, Y. Li, C. Dai and J. Zhu, Aromaticity-promoted CO_2 Capture by P/N-Based Frustrated Lewis Pairs: A Theoretical Study, *Chem. – Asian J.*, 2020, **15**, 266–272.
19 M.-A. Courtemanche, M.-A. Légaré, L. Maron and F.-G. Fontaine, Reducing CO_2 to Methanol Using Frustrated Lewis Pairs: On the Mechanism of Phosphine–Borane-Mediated Hydroboration of CO_2, *J. Am. Chem. Soc.*, 2014, **136**, 10708–10717.
20 M. Faizan and R. Pawar, Boron based intramolecular heterocyclic frustrated Lewis pairs as organocatalysts for CO_2 adsorption and activation, *J. Comput. Chem.*, 2022, **43**, 1474–1483.
21 M. Faizan and R. Pawar, Novel Insight into the Molecular Frustration of IFLPs Based on Boron-Functionalized Pyrimidines for CO_2 Sequestration, *J. Phys. Chem. A*, 2022, **126**, 8633–8644.
22 M. Faizan, K. Saini, R. Mucherla and R. Pawar, Unprecedented Activation of CO_2 by α-Amino Boronic Acids, *J. Phys. Chem. A*, 2023, **127**, 7429–7442.
23 M. Faizan, D. Bana, H. Kumar Gugulothu and R. Pawar, Comparative Investigation on the Catalytic Potential of Borylated Triazine–Based FLPs for CO_2 Sequestration, *ChemistrySelect*, 2024, **9**, e202305133.
24 M. Faizan, G. Santhosh, M. Chakraborty and R. Pawar, *A-Aminodiboronic Acid: A Tri-Functional Frustrated Lewis Pair*

for the Conversion of CO_2 to Value-Added Chemicals, 2024, DOI: 10.2139/ssrn.4753045.

25 R. C. Neu, E. Y. Ouyang, S. J. Geier, X. Zhao, A. Ramos and D. W. Stephan, Probing substituent effects on the activation of H_2 by phosphorus and boron frustrated Lewis pairs, *Dalton Trans.*, 2010, **39**, 4285.

26 S. Guntupalli, M. Faizan, B. S. Bisht and R. Pawar, A comparative study of frustration in Al/P and B/P-based intramolecular frustrated Lewis pairs, *RSC Adv.*, 2025, **15**, 35468–35478.

27 J. J. Cabrera-Trujillo and I. Fernández, Aromaticity-enhanced reactivity of geminal frustrated Lewis pairs, *Chem. Commun.*, 2022, **58**, 6801–6804.

28 J. J. Cabrera-Trujillo and I. Fernández, Aromaticity can enhance the reactivity of P-donor/borole frustrated Lewis pairs, *Chem. Commun.*, 2019, **55**, 675–678.

29 M. Faizan, A. Kumar, M. Raghasudha and R. Pawar, PIO and IBO analysis to unravel the hidden details of the CO_2 sequestration mechanism of aromatically tempered N/B-based IFLPs, *Phys. Chem. Chem. Phys.*, 2023, **25**, 24809–24818.

30 M. Faizan, M. Chakraborty, D. Bana and R. Pawar, Orbital and free energy landscape expedition towards the unexplored catalytic realm of aromatically modified FLPs for CO_2 sequestration, *Phys. Chem. Chem. Phys.*, 2024, **26**, 23609–23622.

31 S. Das, R. C. Turnell-Ritson, P. J. Dyson and C. Corminboeuf, Design of Frustrated Lewis Pair Catalysts for Direct Hydrogenation of CO_2, *Angew. Chem., Int. Ed.*, 2022, **61**, e202208987.

32 S. Das, R. Laplaza, J. T. Blaskovits and C. Corminboeuf, Mapping Active Site Geometry to Activity in Immobilized Frustrated Lewis Pair Catalysts, *Angew. Chem., Int. Ed.*, 2022, **61**, e202202727.

33 F. Bertini, V. Lyaskovskyy, B. J. J. Timmer, F. J. J. De Kanter, M. Lutz, A. W. Ehlers, J. C. Slootweg and K. Lammertsma, Preorganized Frustrated Lewis Pairs, *J. Am. Chem. Soc.*, 2012, **134**, 201–204.

34 B. Jiang, Q. Zhang and L. Dang, Theoretical studies on bridged frustrated Lewis pair (FLP) mediated H_2 activation and CO_2 hydrogenation, *Org. Chem. Front.*, 2018, **5**, 1905–1915.

35 A. M. Spokoyny, C. W. Machan, D. J. Clingerman, M. S. Rosen, M. J. Wiester, R. D. Kennedy, C. L. Stern, A. A. Sarjeant and C. A. Mirkin, A coordination chemistry dichotomy for icosahedral carborane-based ligands, *Nat. Chem.*, 2011, **3**, 590–596.

36 V. N. Kalinin and V. A. Ol'shevskaya, Some aspects of the chemical behavior of icosahedral carboranes, *Russ. Chem. Bull.*, 2008, **57**, 815–836.

37 A. Weller, The two faces of carboranes, *Nat. Chem.*, 2011, **3**, 577–578.

38 T. L. Heying, J. W. Ager, S. L. Clark, D. J. Mangold, H. L. Goldstein, M. Hillman, R. J. Polak and J. W. Szymanski, A New Series of Organoboranes. I. Carboranes from the Reaction of Decaborane with Acetylenic Compounds, *Inorg. Chem.*, 1963, **2**, 1089–1092.

39 M. M. Fein, D. Grafstein, J. E. Paustian, J. Bobinski, B. M. Lichstein, N. Mayes, N. N. Schwartz and M. S. Cohen, Carboranes. II. The Preparation of 1- and 1,2-Substituted Carboranes, *Inorg. Chem.*, 1963, **2**, 1115–1119.

40 J. Aihara, Three-dimensional aromaticity of polyhedral boranes, *J. Am. Chem. Soc.*, 1978, **100**, 3339–3342.

41 R. B. King, Three-Dimensional Aromaticity in Polyhedral Boranes and Related Molecules, *Chem. Rev.*, 2001, **101**, 1119–1152.

42 R. N. Grimes, *Carboranes*, Elsevier, Netherlands, 2011.

43 V. N. Kalinin and V. A. Ol'shevskaya, Some aspects of the chemical behavior of icosahedral carboranes, *Russ. Chem. Bull.*, 2008, **57**, 815–836.

44 R. Hoffmann and W. N. Lipscomb, Theory of Polyhedral Molecules. I. Physical Factorizations of the Secular Equation, *J. Chem. Phys.*, 1962, **36**, 2179–2189.

45 L. I. Zakharkin and V. N. Kalinin, Order of substitution in electrophilic halogenation of barenes (carboranes), *Russ. Chem. Bull.*, 1965, **14**, 1287–1287.

46 L. I. Zakharkin, V. N. Kalinin and N. I. Kobel'kova, On the Specificities of Thermal Isomerization of 3-Substituted 1,2-Dicarba Closo Dodecaboranes(12) into B-Substituted 1,7-Dicarba Closo Dodecaboranes(12), *Synth. React. Inorg. Met.-Org. Chem.*, 1976, **6**, 91–103.

47 M. O. Akram, C. D. Martin and J. L. Dutton, The Effect of Carborane Substituents on the Lewis Acidity of Boranes, *Inorg. Chem.*, 2023, **62**, 13495–13504.

48 A. M. Spokoyny, C. D. Lewis, G. Teverovskiy and S. L. Buchwald, Extremely Electron-Rich, Boron-Functionalized, Icosahedral Carborane-Based Phosphinoboranes, *Organometallics*, 2012, **31**, 8478–8481.

49 J. Schulz, R. Clauss, A. Kazimir, S. Holzknecht and E. Hey-Hawkins, On the Edge of the Known: Extremely Electron–Rich (Di)Carboranyl Phosphines, *Angew. Chem., Int. Ed.*, 2023, **62**, e202218648.

50 L. I. Zakharkin, V. N. Kalinin, A. P. Snyakin and B. A. Kvasov, Effect of solvents on the electronic properties of 1-o-, 3-o- and 1 m-carboranyl groups, *J. Organomet. Chem.*, 1969, **18**, 19–26.

51 M. F. Hawthorne, T. E. Berry and P. A. Wegner, The Electronic Properties of the 1,2- and 1,7-Dicarbaclovododecaborane(12) Groups Bonded at Carbon, *J. Am. Chem. Soc.*, 1965, **87**, 4746–4750.

52 A. Benton, J. D. Watson, S. M. Mansell, G. M. Rosair and A. J. Welch, The Lewis acidity of borylcarboranes, *J. Organomet. Chem.*, 2020, **907**, 121057.

53 J. Zhang and Z. Xie, Tri-insertion with dearomatization of terminal arylalkynes using a carborane based frustrated Lewis pair template, *Chem. Sci.*, 2021, **12**, 1745–1749.

54 C. Dai, Y. Huang and J. Zhu, Predicting Dinitrogen Activation by Carborane-Based Frustrated Lewis Pairs, *Organometallics*, 2022, **41**, 1480–1487.

55 M. Faizan, D. Behera, M. Chakraborty and R. Pawar, Unveiling the Obscure Potential of *O* –Carborane Based

IFLPs for CO_2 Sequestration, *ChemPhysChem*, 2024, e202400647.

56 M. Faizan and R. Pawar, Puppeteering the reactivity of frustrated Lewis pairs toward CO_2 via coordination dichotomy in bridging units, *Phys. Chem. Chem. Phys.*, 2025, **27**, 4587–4592.

57 D. Seyferth, K. D. Buchner, W. S. Rees, L. Wesemann, W. M. Davis, S. S. Bukalov, L. A. Leites, H. Bock and B. Solouki, 1,2-Dimethyl-1,2-disila-closo-dodecaborane(12), a silicon analog of an *o*-carborane: synthesis; X-ray crystal structure; NMR, vibrational, and photoelectron spectra; bonding, *J. Am. Chem. Soc.*, 1993, **115**, 3586–3594.

58 D. Seyferth, K. Büchner, W. S. Rees and W. M. Davis, 1,2-Dimethyl-1,2-disila- *closo*-dodecaborane(12), the First Silicon Analogue of an *ortho*-Carborane, *Angew. Chem., Int. Ed. Engl.*, 1990, **29**, 918–919.

59 L. Wesemann, Y. Ramjoie, M. Trinkaus and B. Ganter, Synthesis and Structure of 1,2-Diphenyl-1,2-disila-closo-dodecaborane(12), Reaction with $[Zr(NMe_2)_4]$ and $[Ta(NMe_2)_5]$, *Z. Anorg. Allg. Chem.*, 1998, **624**, 1573–1576.

60 L. Wesemann, U. Englert and D. Seyferth, First Reaction of 1,2-Dimethyl-*o*-silaborane: Nucleophilic Degradation, *Angew. Chem., Int. Ed. Engl.*, 1995, **34**, 2236–2238.

61 L. Wesemann, M. Trinkaus, Y. Ramjoie, B. Ganter, U. Englert and J. Müller, Adducts ofo-Silaborane With Water and Methanol, *Eur. J. Inorg. Chem.*, 2000, **2000**, 735–739.

62 K. B. Wiberg, Ab Initio Molecular Orbital Theory by W. J. Hehre, L. Radom, P. v. R. Schleyer, and J. A. Pople, John Wiley, New York, Price: $79.95, 1986, 548 pp, *J. Comput. Chem.*, 1986, **7**, 379.

63 J.-D. Chai and M. Head-Gordon, Long-range corrected hybrid density functionals with damped atom–atom dispersion corrections, *Phys. Chem. Chem. Phys.*, 2008, **10**, 6615–6620.

64 M. J. Frisch, G. W. Trucks, H. B. Schlegel, G. E. Scuseria, M. A. Robb, J. R. Cheeseman, G. Scalmani, V. Barone, G. A. Petersson, H. Nakatsuji, X. Li, M. Caricato, A. V. Marenich, J. Bloino, B. G. Janesko, R. Gomperts, B. Mennucci, H. P. Hratchian, J. V. Ortiz, A. F. Izmaylov, J. L. Sonnenberg, D. Williams-Young, F. Ding, F. Lipparini, F. Egidi, J. Goings, B. Peng, A. Petrone, T. Henderson, D. Ranasinghe, V. G. Zakrzewski, J. Gao, N. Rega, G. Zheng, W. Liang, M. Hada, M. Ehara, K. Toyota, R. Fukuda, J. Hasegawa, M. Ishida, T. Nakajima, Y. Honda, O. Kitao, H. Nakai, T. Vreven, K. Throssell, J. A. Montgomery Jr., J. E. Peralta, F. Ogliaro, M. J. Bearpark, J. J. Heyd, E. N. Brothers, K. N. Kudin, V. N. Staroverov, T. A. Keith, R. Kobayashi, J. Normand, K. Raghavachari, A. P. Rendell, J. C. Burant, S. S. Iyengar, J. Tomasi, M. Cossi, J. M. Millam, M. Klene, C. Adamo, R. Cammi, J. W. Ochterski, R. L. Martin, K. Morokuma, O. Farkas, J. B. Foresman and D. J. Fox, *Gaussian 16 Rev. C.01*, Gaussian, Inc., Wallingford, CT, 2016.

65 R. F. W. Bader, Atoms in molecules, *Acc. Chem. Res.*, 1985, **18**, 9–15.

66 R. F. W. Bader, *Atoms in Molecules: A Quantum Theory*, Oxford University Press, Oxford, 1990.

67 *The Quantum Theory of Atoms in Molecules: From Solid State to DNA and Drug Design*, ed. C. F. Matta and R. J. Boyd, Wiley, 1st edn, 2007.

68 T. Lu and F. Chen, Multiwfn: A multifunctional wavefunction analyzer, *J. Comput. Chem.*, 2012, **33**, 580–592.